Journal of Molecular Structure 984 (2010) 30–38

Contents lists available at ScienceDirect

Journal of Molecular Structure

journal homepage: www.elsevier.com/locate/molstruc

Synthesis, characterization, DNA binding and cleavage studies of Ru(II) complexes containing oxime ligands

Nataraj Chitrapriya [a], Viswanathan Mahalingam [b], Matthias Zeller [c], Hyosun Lee [a], Karuppannan Natarajan [b,*]

[a] Department of Chemistry, Kyungpook National University, 1370 Sankyuk-dong, Buk-gu, Deagu-city 702-701, Republic of Korea
[b] Department of Chemistry, Bharathiar University, Coimbatore 641 046, India
[c] Department of Chemistry, Youngstown State University, Youngstown, OH 44555-3663, USA

ARTICLE INFO

Article history:
Received 9 June 2010
Received in revised form 27 August 2010
Accepted 1 September 2010
Available online 24 September 2010

Keywords:
Ru(II) oxime complexes
Oximato oxygen
X-ray crystal structures
Electrochemistry
DNA binding and cleavage

ABSTRACT

The Ru(II) precursors, $[RuHCl(CO)(EPh_3)_3]$ (E = P or As) when reacted with some well known monoxime and dioxime ligands in ethanolic solution afforded the new complexes of the types $[RuCl(CO)(EPh_3)_2L1]$, $[RuH(CO)(EPh_3)_2L2]$ and $[RuCl(CO)(EPh_3)_2L3]$ ((H_1L1) = diacetylmonoxime, (H_1L2) = dimethylglyoxime and (H_2L3) = benzoiloxime). The ligands coordinated in a bidentate chelate mode forming a five membered chelate ring. The molecular structures of two of the complexes have been determined by single crystal X-ray diffraction study. The structural determination confirms the deprotonation of the oxime function. Examination of all the complexes by cyclic voltammetry showed the occurrence of some quasi-reversible redox reactions owing to changes in the oxidation state of the central metal atoms. Structural assignments are supported by combination of IR, UV–Vis, ^1H NMR and elemental analyses. In addition, the DNA binding properties and cleavage efficiency of new complexes have been tested.

1. Introduction

Organometallic and coordination chemistries of oximes constitute an active area of research, with efforts in particular being directed toward unusual reactivity modes of oximes and their complexes [1–3]. One potential advantage to the use of oximes is the possibility of greater tunability by facile variation of the substituents [4]. The presence of mild acidic hydroxyl groups and slightly basic nitrogen atoms makes oximes amphoteric ligands [5–8]. Nitrogen coordination of the oxime group to a metal ion leads to a dramatic increase in its acidic character and formation of an oximato ligand is favored [9]. The binding mode of the oxime group depends to a great extent not only on the nature of the metal ion but on the presence of a neighboring donor group in the same ligand. The combination of these two moieties results in stable chelate rings upon coordination to a metal ion [10]. Traditionally, oximes have been extensively used in analytical chemistry and metallurgy as very effective complexing agents for the purposes of isolation, separation and extraction of different metal ions. Molecular design of multidonor ligands containing other strong donor groups along with the oxime function may lead to new, very effective chelating agents [11]. The capacity of the oximato group to coordinate additional metal ions via the bridging N and O functions and the fact that the oxime bridges were established to mediate exchange interactions between paramagnetic centers very effectively provoked the start of a wide usage of oxime ligands in molecular magnetism for the design and synthesis of polynuclear assemblies [12,13].

Oximes and their metal complexes are of current interest for their rich physicochemical properties, reactivity patterns and potential applications in many important chemical processes in the areas of medicine [14–16], bioorganic systems [17,18], catalysis [19], electrochemical [20] and electro optical sensors [21,22]. The investigations of the redox properties of these types of complexes are also of great interest in terms of their various technological applications [23–25]. The interest in oxime containing coordination compounds is constantly increasing in connection with the biological implication of oximes (especially, as intermediates in the biosynthesis of nitrogen oxide) and the marked and versatile bioactivity indicated by different oximes and their metal complexes [26]. It is important to note that the realization of the biological function of oximes and the mechanism of their metabolism in living systems are evidently connected with their chelation by metal ions [27]. Ruthenium(II) complexes have shown to act not only as good catalysts for many industrially important reactions but also have shown promising biological activities including anticancer activities [14]. Hence, there is a need for the synthesis of oxime complexes of ruthenium(II) and to study their reactivities. Herein, we report the synthesis, characterization,

* Corresponding author. Tel.: +91 422 2428311; fax: +91 422 2422387.
E-mail address: k_natraj6@yahoo.com (K. Natarajan).

0022-2860/$ - see front matter © 2010 Elsevier B.V. All rights reserved.
doi:10.1016/j.molstruc.2010.09.004

electron transfer and DNA binding properties of Ru(II) oxime complexes. Also the DNA cleavage properties have been studied using pBR322 super coiled plasmid DNA.

2. Experimental

2.1. Materials and methods

All chemicals were of reagent grade and were used without further purification. Solvents were purified and dried according to standard procedures [28]. The ruthenium(II) precursor complexes $[RuHCl(CO)(PPh_3)_3]$ and $[RuHCl(CO)(AsPh_3)_3]$ were prepared by reported literature methods [29,30]. All the ligands are obtained from commercial suppliers and were used as received. Protein free Herring Sperm ds DNA obtained from SRL chemicals was stored at 0–4 °C and its purity was checked by measuring the optical density before use. The pBR322 plasmid DNA was purchased from Amersham–Pharmacia Biotech. Ultra-pure MilliQ water (18.2 mΩ) was used in experiments. The Tris-buffer solution was prepared with double-distilled water and its pH was adjusted to 7.1 using 0.1 M NaOH solution. DNA stock solutions were freshly prepared with this buffer solution before use. Distilled dimethyl sulphoxide (DMSO) was used for the preparation of solutions of complexes for DNA-binding studies. Commercially available TBAP (tetra butyl ammonium perchlorate) was properly dried and used as supporting electrolyte for recording cyclic voltammograms of the complexes (except for DNA-binding studies). FT-IR spectra (4000–400 cm^{-1}) of the complexes and the free ligands were recorded as KBr pellets with a Nicolet Avatar Model FT-IR spectrophotometer. UV–Vis spectra (800–250 nm) of the complexes were obtained on a Systronics 119 UV–Vis spectrophotometer. ^1H NMR spectra of the complexes were recorded using a Varian-Australia AMX-400 spectrometer. Micro analyses (C, H & N) were performed on a Vario EL III Elementar analyzer. Cyclic voltammograms were recorded on CHI 1120A electrochemical analyzer with a three electrode compartment consisting of a platinum disc working electrode, platinum wire counter electrode and Ag/Ag^+ reference electrode.

2.2. X-ray crystallography

X-ray diffraction measurements were performed on a Bruker AXS SMART APEX CCD diffractometer with graphite monochromatized Mo Kα radiation. The unit cell was determined using SMART [31], SAINT+ [32] and the data were corrected for absorption using SADABS [33]. The structure was solved by direct methods and refinements were carried out by full-matrix least-square techniques. The hydrogen atoms were treated by a mixture of independent and constrained refinement. The computer program SHELXTL 6.14 [34] was used for structure solution, refinement and molecular graphics. Refinement of an extinction coefficient was found to be insignificant. All non-hydrogen atoms were refined anisotropically.

2.3. DNA binding experiments

The experiments were carried out in Tris–HCl buffer (50 mM, pH 7.1) using a solution of Herring sperm DNA which gave a UV absorbance at 260 and 280 nm in a 1.8:1 ratio indicating that the DNA is sufficiently free from protein. No further effort was made to purify the commercially obtained DNA. The concentration of DNA was determined by absorption spectroscopy using the ε value of 6600 M^{-1} cm^{-1} at 260 nm. DNA melting experiments were carried out by monitoring the absorption (260 nm) of HS-DNA at various temperatures in the absence and presence of the complexes at 1:1 ratio with ramp rate of 0.1 °C/min. The viscosity measurement was carried out using an Ubbelodhe viscometer immersed in a thermostatic water bath maintained at 16(±0.l) °C. DNA samples with approximately 200 base pairs in length were prepared by sonication in order to minimize complexities arising from DNA flexibility. Flow times were measured with a digital stopwatch; each sample was measured three times, and an average flow time was calculated. Relative viscosities for HS-DNA in the presence and absence of the complex were calculated from the relation $\eta = (t - t_0)/t_0$, where t is the observed flow time of DNA-containing solution and t_0 is the flow time of Tris–HCl buffer alone. Data are presented as $(\eta/\eta_0)^{1/3}$ versus binding ratio, where η is the viscosity of HS-DNA in the presence of complex and η_0 is the viscosity of HS-DNA alone. For the gel electrophoresis experiment, supercoiled pBR322 DNA (0.1 μg) was treated with the Ru(II) complexes in the presence of oxygen and sodium ascorbate (1 mM) in Tris–HCl buffer (50 mM) with 0.1 M NaCl (pH, 7.1) followed by dilution with the Tris–HCl buffer to a total volume of 20 μl. The samples were incubated for 24 h at 37 °C. A loading buffer containing 25% bromophenol blue, 0.25% xylene cyanol, 30% glycerol (3 μl) was added and electrophoresis performed at 100 V for 2 h in Tris–Acetate–EDTA (TAE) buffer using 1% agarose gel containing 1.0 μg/ml ethidium bromide. Agarose gel electrophoresis of plasmid DNA was visualized by photographing the fluorescence of intercalated ethidium bromide under a UV illuminator. The cleavage efficiency was measured by determining the ability of the complex to convert the supercoiled DNA (SC) to nicked circular form (NC) and linear form.

2.4. Synthesis of new Ru(II) oxime complexes

All the complexes were synthesized by the following general method. To a suspension of the appropriate oxime ligand (0.1 mmol) in ethanol (30 cm^3) was added the respective Ru(II) starting complex (0.1 mmol). The resulting solution was refluxed for 10 h. On slow evaporation at room temperature, the product got separated which was filtered and washed with diethyl ether and cold ethanol.

2.4.1. $[RuCl(CO)(PPh_3)_2(L1)]$ (**1**)

It was prepared from $[RuHCl(CO)(PPh_3)_3]$ (0.1 g, 0.105 mmol) and diacetylmonoxime (0.0105 g, 0.105 mmol) as an orange crystalline product. Yield: 48 mg (68%). Anal. Calc. for $C_{41}H_{36}O_3N_1RuClP_2$: C, 62.39; H, 4.59; N, 1.77. Found: C, 62.31; H, 4.53; N, 1.75%. IR (KBr, cm^{-1}): ν(C=O) 1642, ν(C=N) 1577, ν(N–O) 974. ^1H NMR (400 MHz, $CDCl_3$, δ, ppm; s, singlet; m, multiplet): 1.65 (s, 3H, CH_3), 1.70 (s, 3H, CH_3), 7.26–7.68 (m, aromatic). UV–Vis λ (nm) (ε, mol^{-1} cm^{-1} L): 229(29,649), 259(19,115), 416(1509).

2.4.2. $[RuH(CO)(PPh_3)_2(HL2)]$ (**2**)

It was prepared from $[RuHCl(CO)(PPh_3)_3]$ (0.1 g, 0.105 mmol) and dimethylglyoxime (0.0121 g, 0.105 mmol) as an yellow crystalline product. Yield: 51 mg (70%). Anal. Calc. for $C_{41}H_{38}O_3N_2RuP_2$: C, 63.97; H, 4.97; N, 3.63. Found: C, 63.58; H, 4.58; N, 3.68%. IR (KBr, cm^{-1}): ν(C=N) 1625, ν(N–O) 930. ^1H NMR(400 MHz, $CDCl_3$, δ, ppm; s, singlet; m, multiplet): 2.85 (s, 3H, CH_3), 2.95 (s, 3H, CH_3), 7.24–7.71 (m, aromatic), 9.30 (s, 1H, N–OH). UV–Vis λ (nm) (ε, mol^{-1} cm^{-1} L): 227(41,054), 228(41,955), 269(13,129).

2.4.3. $[RuCl(CO)(PPh_3)_2(L3)]$ (**3**)

It was prepared from $[RuHCl(CO)(PPh_3)_3]$ (0.1 g, 0.105 mmol) and benzoinoxime (0.0239 g, 0.105 mmol) as purple color product. Yield: 62 mg (58%). Anal. Calc. for $C_{51}H_{41}O_3N_1RuClP_2$: C, 66.99; H, 4.51; N, 1.53. Found: C, 66.79; H, 4.55; N, 1.59%. IR (KBr, cm^{-1}): ν(C=N) 1598, ν(C–O) 1375, ν(N–O) 932. ^1H NMR (400 MHz, $CDCl_3$, δ, ppm; s, singlet; m, multiplet): 6.8 (s, 1H, CH–), 7.20–7.70 (m,

aromatic). UV–Vis λ (nm) (ε, $mol^{-1}\,cm^{-1}\,L$): 223(25,770), 263(8464), 552(694).

*2.4.4. [RuCl(CO)(AsPh$_3$)$_2$(L1)] (**4**)*

It was prepared from [RuHCl(CO)(AsPh$_3$)$_3$] (0.1 g, 0.107 mmol) and diacetylmonoxime (0.0107 g, 0.107 mmol) as red color product. Yield: 53 mg (67 %). Anal. Calc. for $C_{41}H_{36}O_3N_1RuClAs_2$: C, 56.14; H, 4.13; N, 1.59. Found: C, 56.21; H, 4.32; N, 1.59%. IR (KBr, cm^{-1}): ν(C=O) 1639, ν(C=N) 1577, ν(N–O) 987. ^{1}H NMR (400 MHz, $CDCl_3$, δ, ppm; s, singlet; m, multiplet): 1.60 (s, 3H, CH_3), 1.75 (s, 3H, CH_3), 7.26–7.56 (m, aromatic). UV–Vis λ (nm) (ε, $mol^{-1}\,cm^{-1}\,L$): 228(20,198), 260(18,911), 303(3754), 425(1024).

*2.4.5. [RuH(CO)(AsPh$_3$)$_2$(HL2)] (**5**)*

It was prepared from [RuHCl(CO)(AsPh$_3$)$_3$] (0.1 g, 0.107 mmol) and dimethylglyoxime (0.0124 g, 0.107 mmol) as an yellow product. Yield: 49 mg (61%). Anal. Calc. for $C_{41}H_{38}O_3N_2RuAs_2$: C, 57.41; H, 4.46; N, 3.26. Found: C, 57.86; H, 4.64; N, 3.38%. IR (KBr, cm^{-1}): ν(C=N) 1617, ν(N–O) 923. ^{1}H NMR 400 MHz, $CDCl_3$, δ, ppm; s, singlet; m, multiplet): 2.85 (s, 3H, CH_3), 2.95 (s, 3H, CH_3), 7.00–7.70 (m, aromatic), 9.60 (s, 1H, N–OH). UV–Vis λ (nm) (ε, $mol^{-1}\,cm^{-1}\,L$): 230(9833), 245(9649), 256(28,275), 379(1358).

*2.4.6. [RuCl(CO)(AsPh$_3$)$_2$(L3)] (**6**)*

It was prepared from [RuHCl(CO)(AsPh$_3$)$_3$] (0.1 g, 0.107 mmol) and benzoinoxime (0.0249 g, 0.107 mmol) as purple product. Yield: 76 mg (67%). Anal. Calc. for $C_{51}H_{41}O_3N_1RuClAs_2$: C, 61.11; H, 4.12; N, 1.39. Found: C, 61.17; H, 4.14; N, 1.38%. IR (KBr, cm^{-1}): ν(C=N) 1605, ν(C–O) 1381 ν(N–O) 932. ^{1}H NMR (400 MHz, $CDCl_3$, δ, ppm; s, singlet; m, multiplet): 6.8 (s, 1H, CH–), 7.20–7.80 (m, aromatic). UV–Vis λ (nm) (ε, $mol^{-1}\,cm^{-1}\,L$): 227(13,726), 267(7048), 536(880).

3. Results and discussion

The starting complexes of general formula [RuHCl(CO)(EPh$_3$)$_3$] (where E = As or P) were reacted with three oxime ligands [(H_1L1) = diacetylmonoxime, (H_2L2) = dimethylglyoxime and (H_2L3) = benzoinoxime]. The primary intension of the present study has been to see how the oxime ligands interact with Ru(II) complexes. Three types of complexes have been obtained (Scheme 1) and they have been characterized by spectroscopic techniques. The elemental analyses data confirm the molecular formulae of the complexes. The oxime ligands coordinate to ruthenium ion as a bidentate donor forming a five membered chelate ring leaving the oximato oxygen atom uncoordinated. All the six complexes synthesized are diamagnetic. Structures of two of the complexes have been determined by single crystal X-ray crystallography.

3.1. IR spectra

The IR spectral data are given experimental section and are discussed below in terms of the pertinent regions of the spectrum. Generally oximes are characterized by three IR absorption bands due to ν(O–H), ν(C=N) and ν(N–O) stretching vibrations [35]. The IR spectra of all the ligands exhibit a broad medium intensity band around 3250 cm^{-1}, which is assigned to ν(O–H) of the oxime group. The bands in the region 976–1018 cm^{-1} and 1590–1641 cm^{-1} are due to ν(N–O) and ν(C=N) respectively. In case of HL1 alone, a strong peak at 1671 cm^{-1} due to ν(C=O) moiety has been observed. The striking feature common in all the spectra of the complexes are the noticeable shift of ν(N–O) and ν(C=N) stretching vibrations relative to the free ligands. This suggests the coordination of the oxime group through nitrogen atom in all the complexes. In the spectra of complexes (**1**) and (**4**), the ν(C=O) band is shifted to lower frequencies by about 30 cm^{-1} compared to free ligands, indicating the coordination of oxygen atom of the carbonyl moiety to Ru(II) ion. In the spectra of (**2**) and (**5**), the band due to ν(OH) appeared around 2500 cm^{-1} instead of around 3200 cm^{-1} indicating the hydrogen bonding between the hydroxyl group and the oxygen atom of DMF molecule. Normally hydrogen bonded hydroxyl groups are found to absorb at lower energy depending on the extent of hydrogen bonding. The presence of hydrogen bonding has also been reflected from the decrease in ν(N–O) frequency observed in the IR spectra of complexes. This is also confirmed by the shift in N–O absorbance to lower energy. This decrease is consistent with protonation occurring at a hydrogen bonded oxime oxygen atom, in that such a protonation would be expected to result in a removal of electron density from the N–O bond and a corresponding increase in the N–O bond length and a decrease in N–O stretching frequency. The expected increase of an N–O bond length upon the formation of a covalent O–H bond associated with oxime oxygen has been confirmed by X-ray structural determination of complex (**2**). The absorption band which appeared at 2020 cm^{-1} has been assigned to ν(Ru–H) for the hydrido complexes (**2** and **5**). However, this band was not observed for the other complexes (**1**, **3**, **4** and **6**). The IR spectrum of benzoiloxime showed a band at 1388 cm^{-1} and band at 3480 cm^{-1} due to ν(C–O) and ν(OH) respectively. In the spectra of (**3**) and (**6**), the band at 3480 cm^{-1} has completely disappeared indicating the deprotonation of –OH prior to coordination. This coordination by oxygen atom has been further confirmed by the reduction in ν(C–O) to around 1375 cm^{-1}. Characteristic band for ν(OH) of (N–OH) group is absent in the spectra of all the complexes indicating the deprotonation of N–OH group.

3.2. Electronic spectra

The electronic spectra of all the new complexes have been recorded in $CHCl_3$ solution. The spectral data are given in the experimental section. The low spin d^6 complexes are generally dominated by metal to ligand charge transfer in the visible region [36,37]. All the complexes display three to four absorptions, one of which appears in the visible region while the others extended into the UV region. The bands in the region 379–552 nm have been assigned to the metal–ligand charge transfer transition on the basis of high extinction coefficient values. Two to three high energy bands which appeared around 223–303 nm in all the complexes are attributed tintraligand (oxime) $\pi \rightarrow \pi^*$ transition [38].

3.3. ^{1}H NMR spectra

^{1}H NMR spectra of complexes were recorded in $CDCl_3$, and their assignments are given in the experimental section. The spectra of the complexes (**1**) and (**4**) showed two singlet, one at δ 1.60–1.63 ppm and the other at δ 1.70–1.75 ppm, attributed to the resonance of the two magnetically different methyl groups. The complexes (**2**) and (**5**) displayed two singlets at δ 2.85 and δ 2.95 ppm, which are assigned to the two different methyl protons of the ligand (H_2L2). The methyl groups in (H_2L2) are known to be non equivalent [39,40]. For the complexes (**2**) and (**5**), a singlet at δ 9.2 and δ 9.4 ppm have been observed respectively for the N–OH proton. However, the spectra of the complexes **1**, **3**, **4** and **6** did not show any signal for N–OH indicating the deprotonation of oxime proton leaving oximato oxygen uncoordinated (crystal structure will be discussed later). The metal hydride signal corresponding to Ru–H has been detected as a singlet at δ −12.3 ppm for the complexes (**2** and **5**). However, this peak was not observed for the complexes (**1**, **3**, **4** and **6**). The >CH proton of >CHOH which appeared at δ 5.6 ppm for benzoinoxime ligand (H_2L3) has been

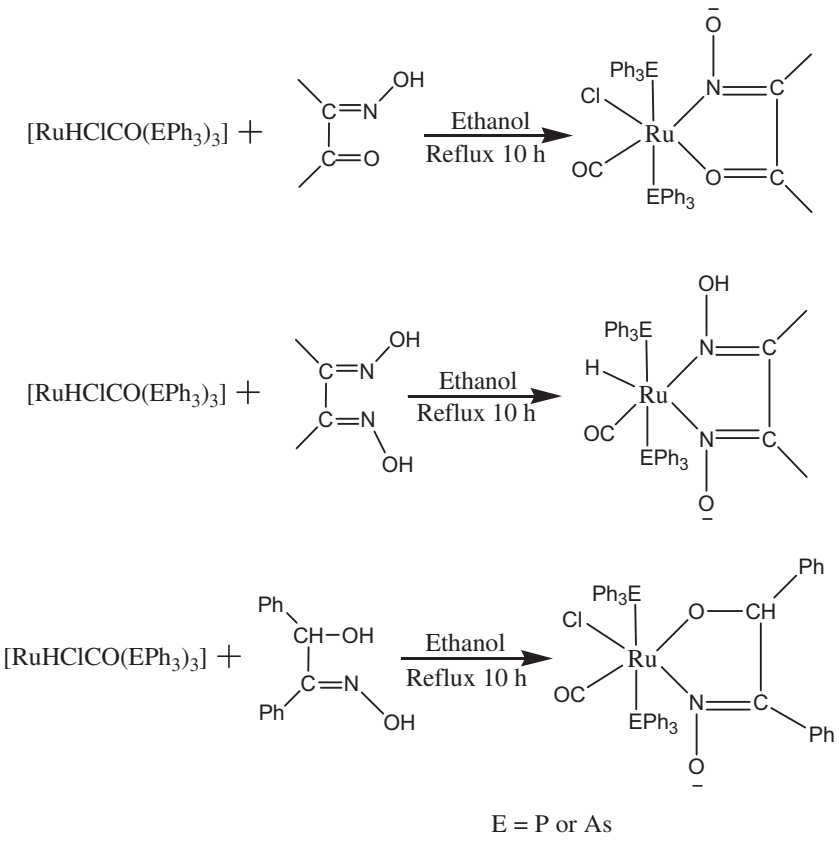

Scheme 1.

shifted to δ 6.8 ppm in the complexes (**3**) and (**6**) indicating its deshielding due to the coordination of oxygen to the metal ion. The aromatic protons appeared as a multiplet in the region δ 6.9–8.0 ppm in all the complexes.

3.4. X-ray structure determination

The molecular structures of (**1**) and (**2**) are illustrated in Figs. 1 and 2 respectively and their pertinent crystallographic data are listed in Table 1. The significant bond distance and angles of the complexes are given in Table 2. In (**1**), Ru(II) ion is coordinated to carbonyl oxygen and oxime nitrogen of the ligand (H_1L1) forming a five membered chelate ring with a bite angle of 78.25(5)°. The ruthenium atom is hexacoordinated with slightly distorted octahedral geometry. The two P atoms from triphenylphosphine occupy the apical position while one chloride, carbon atom from carbonyl group and oxygen and nitrogen atoms of the ligand occupy basal plane of the octahedron. The bond distances Ru1–N1 and Ru1–O1 therein are 2.0100(14) Å and 2.1041(12) Å respectively, which are about the same length as those found in related Ru(II) complexes [41–43]. The Ru–Cl, Ru–C and Ru–P distances are all normal and they are similar to what have been observed in structurally characterized Ru(II) complexes containing these bonds [42,44,45]. The geometrical parameters of the present ligand are similar to those observed for other ligands having deprotonated oxime group [41,42]. The distance N1–O1 of 1.2577(19) Å and N1–C3 of 1.362(2) Å are close to reported values of nitrogen coordinated deprotonated oxime group [41,46,47]. Loss of the N–OH hydrogen and coordination of the oxime nitrogen results in significant decreases in the N1–O1 bond distance compared to the protonated N–O bond distance found in reported oxime complexes [41,48]. The bond distances of C3–C4 and C3–C2 have been found to be shorter due to deprotonation of oxime OH. It has been noted that N–O distances in oxime complexes are sensitive indicators of

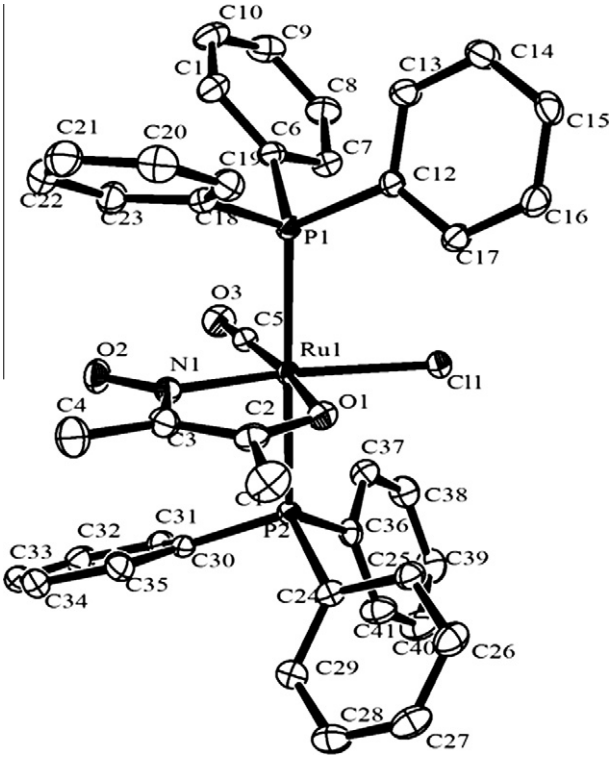

Fig. 1. Labeled ORTEP diagram of (**1**) with thermal probability. Hydrogen atoms are omitted for clarity.

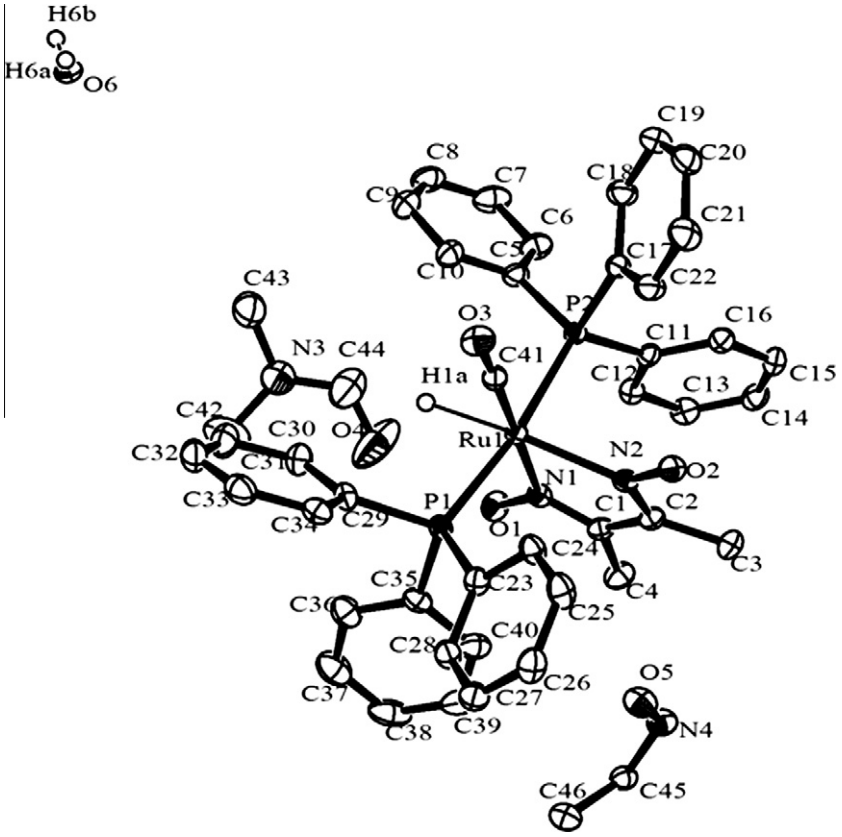

Fig. 2. Labeled ORTEP diagram of (**2**) with thermal probability. Hydrogen atoms are omitted for clarity.

Table 1
Crystal data for (**1**) and (**2**).

Crystal data	(**1**)	(**2**)
Empirical formula	$C_{41}H_{36}ClNO_3P_2Ru$	$C_{46}H_{51}N_4O_6P_2Ru$
Formula weight	789.17	918.92
Crystal color, Habit	Orange, Block	Yellow, Block
Crystal dimensions	0.37 × 0.36 × 0.34mm	0.45 × 0.35 × 0.22mm
Crystal system	Monoclinic	Triclinic
Lattice type	Primitive	Primitive
Space group	*P2(1)/n*	*P-1*
A	9.9789(7) Å	10.6021(4)
B	16.1803 (11) Å	12.5182(5)
C	22.6705 (15) Å	17.3708(7)
α	90°	83.1850(10)
β	95.6050 (16)°	89.0220(10)
γ	90°	69.8710(10)
V	3642.9 (4) Å^3	2148.63(15)
Z	4	2
Reflections collected	30070	22527
Unique reflections	8902	10633
Reflections [$I > 2\sigma(I)$]	8352	9594
R [$F^2 > 2\sigma(F^2)$]	0.0290	0.0343
wR [F^2]	0.0734	0.0920
D_{calc}	1.439 Mg m^{-3}	1.420
F_{000}	1616	954
μ (Mo Kα)	0.631 mm^{-1}	0.493
R_{int}	0.0216	0.0181
Goodness of fit (*S*)	1.056	1.043
θ_{max} (°)	30.53	30.54

Table 2
Selected bond lengths (Å) and bond angles (°) for (**1**) and (**2**).

(**1**)		(**2**)	
Ru1–C5	1.8668(19)	Ru1–C41	1.8484(19
Ru1–N1	2.0100(14)	Ru1–N1	2.1001(15)
Ru1–O1	2.1041(12)	Ru1–N2	2.1602(15)
Ru1–Cl1	2.4384(4)	Ru1–H1A	1.84(2)
Ru1–P1	2.3943(4)	Ru1–P1	2.3461(5)
Ru1–P2	2.3819(4)	Ru1–P2	2.3678(5)
C5–Ru1–Cl1	96.43(5)	C51–Ru1–C50	95.2(2)
C5–Ru1–N1	94.48(7)	C51–Ru1–N3	170.9(4)
C5–Ru1–O1	172.72(6)	C51–Ru1–O2	100.7(3)
C5–Ru1–P1	91.11(5)	C51–Ru1–P1	92.4(4)
C5–Ru1–P2	89.15(5)	C51–Ru1–P2	87.5(4)
N1–Ru1–Cl1	168.98 (4)	C50–Ru1–N3	78.1(4)
N1–Ru1–O1	78.25(5)	C50–Ru1–O2	163.8(2)
N1–Ru1–P1	89.93(4)	C50–Ru1–P1	90.98(18)
N1–Ru1–P2	90.85(3)	C50–Ru1–P2	89.1(7)
O1–Ru1–Cl1	90.84(4)	N3–Ru1–O2	85.8(4)
O1–Ru1–P1	89.01(3)	N3–Ru1–P1	87.8(4)
O1–Ru1–P2	90.85(3)	N3–Ru1–P2	92.4(4)
P2–Ru1–Cl1	87.663(14)	O2–Ru1–P1	91.28(18)
P2–Ru1–P1	179.064(15)	O2–Ru1–P2	88.73(18)
P1–Ru1–P2	91.413(14)	P1–Ru–P2	179.81(4)

the deprotonation of the hydrogen atom and position of the hydrogen atom (covalently or hydrogen bonded). The observation of shorter N–O bond length and larger C–N–O angles definitively rule out the possibility of oxime protons being present in the complexes.

The coordination geometry of (**2**) is best described as distorted octahedron with two nitrogen atoms from chelating ligand, C atom from CO and hydride ion occupying the four equatorial positions and two PPh_3 molecules filling the axial sites. The structure shows that the ligand (H_2L2) is coordinated to ruthenium through the two oxime nitrogen atoms, forming a five membered chelate ring with a bite angle of N1–Ru1–N2 = 74.81(16)°. The two trans PPh_3 ligands have been found to bent away from the coordinated H_2L2 ligand [P1–Ru1–P2 = 172.26(17) Å] due to steric bulk of the chelated H_2L2. This has resulted in lowering of angle for P2–Ru1–C41 =

89.23(6)° and P1–Ru1–H1A = 82.0(7)° compared P1–Ru1–N1 = 91.00(4)° and P2–Ru1–N2 = 89.12(4)° angles. The Ru–P, Ru–H, Ru–C bond lengths are quite normal and they are comparable with the values reported for other complexes [49–51]. It is interesting to note that though the ligand (H_2L2) consists of two dissociable oxime protons, only one of the oxime protons is deprotonated during complexation. The Ru1–N1 bond length 2.1001(15) Å is shorter than Ru1–N2 [2.1602(15) Å] length. Generally, the M–N(oxime) distances are related to the N–O bond distances, which are in turn, allied to the protonation or nonprotonation of oxygen. The Ru–N length on the protonated side of glyoxime is significantly shorter than those on the deprotonated side. In support of the above conclusion, we note that the two N–O distances are significantly different (they are being 1.3914(19) Å and 1.3299(19) Å for N1–O1 and N2–O2 respectively), the longer N–O distance is associated with the oxygen atom which is covalently bound to the hydrogen atom. The bond distances of C=N and C–CH3 also show the effect of the deprotonation. The C2–N2 bond length is 1.302(2) Å, which is an intermediate value between single and double bond lengths and C2–C3 distance of 1.320 Å is significantly shorter. These are in sharp contrasts to what was found for protonated side and free glyoxime ligand. The above facts suggest a delocalization of the π electron density on deprotonated side of the glyoxime (O2–N2–C2–C3) moiety. The observed distances of C1–N1 = (1.298(2) Å) and C1–C4 = (1.502(3) Å) are in agreement with those distances found in the free ligand [52]. The shortening of the N–O distance and lengthening of the C–N distance in the oxime group are characteristic of oxime donor ligands and were observed earlier in the relevant structures [53,54]. The structure is additionally stabilized by the formation of hydrogen bonding. One of the oxygen bound acidic hydrogen atom is lost from the ligand during complex formation and remaining hydroxyl group of the ligand is involved in hydrogen bonding to the oxygen (O4) atom from the DMF of crystallization. Both hydrogen atoms of the water molecule are participating in hydrogen bonding (Table 3). Atom O2 forms a bifurcated hydrogen bond, with H6A and H6B of water molecule. In addition to that, the free ligand (H_2L2) present in the crystal lattice is also found to participate in the intermolecular hydrogen bonding. The hydrogen bond is formed between O5 of the free ligand and O6 of solvent water.

3.5. Cyclic voltammetry

Electrochemical properties of the complexes have been studied by cyclic voltammetry. Voltammetric data are presented in Table 4 and a representative voltammogram is displayed in Fig. 3. Each complex shows one oxidative and two reductive responses. The cyclic voltammograms of all the complexes are dominated by the Ru(II)–Ru(III) redox couple. The complexes (**1**) and (**4**) showed irreversible redox behaviour, whereas (**2**), (**3**), (**5**) and (**6**) showed reversible redox behaviour with peak to peak separation in the range 70–80 mV. Comparison of the peak potential of the ligands with those of the complexes reveals that the two reductive responses are ligand centered reduction. From the electrochemical data, it is inferred that the present ligand system is ideally suitable for stabilizing the Ru(II) ion.

Table 3
Hydrogen bonding geometry for (**2**).

D–H···A	D–H	H···A	D···A	D–H···A
(**1**)				
O1 H1 O4	0.84	1.81	2.602(3)	156(1)
O5 H5 O6	0.84	1.85	2.686(2)	175(5)
O6 H6AO2	0.833	2.028	2.8494(19)	169(3)
O6 H6BO2	0.813	1.921	2.7320(19)	176(3)

Table 4
Cyclic voltammetry data for Ru(II) complexes.

Complex	Ru(III)/Ru(II)[a] $E_{1/2}/V(\Delta Ep/mV)$	Ligand reduction	
(**1**)	1.4[b]	−1.27(390)	−1.5[c]
(**2**)	1.07(160)	−1.19(50)	−1.5[c]
(**3**)	0.82(540)	−1.21(230)	−1.51[c]
(**4**)	1.48[b]	−1.28(370)	−1.5[c]
(**5**)	1.09(80)	−1.22(110)	−1.5[c]
(**6**)	1.06(110)	−1.18(170)	−1.45[c]

[a] Oxidation couple.
[b] Irreversible, Ep_a value.
[c] irreversible, Ep_c value.

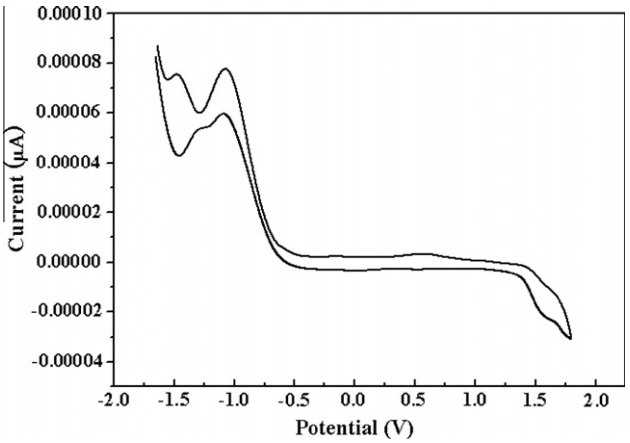

Fig. 3. Cyclic voltammogram of complex (**1**).

3.6. DNA-binding studies

3.6.1. Absorption spectroscopic studies

DNA-binding studies are important for the rational design and construction of new and more efficient drugs targeted to DNA. Electronic absorption spectroscopy is often employed to ascertain the binding of complexes with DNA. The spectral change reflects the corresponding changes in DNA in its conformation and structures after the drug bound to DNA. The extent of spectral change is related to the strength of binding [55,56]. Hypochromism results from the contraction of DNA in the helix axis, as well as from the change in conformation in DNA, in contrast hyperchromism derives from damage to the DNA double helix structure [57,58]. The spectra of all complexes consist of two to three resolved bands. The MLCT band of complexes (**1**) and (**4**) at 438 and 442 nm respectively showed clearly that the progressive addition of DNA to the complexes leads to strong hyperchromism, accompanied the slight red shifts of 3 nm and 1 nm respectively The extent of hyperchromism (53%) in (**1**) is higher at saturation point than that observed for (**4**). A strong hyperchromic effect with significant red shift was observed for (**1**), suggesting that this complex possesses a higher propensity for DNA binding. The other bands at 261 and 259 nm experience a slight blue shift, a change in band shape and hyperchromism. The hyperchromism of the complexes implies that the binding mode is non-intercalative in nature. With increasing concentration of DNA, the absorption bands of (**2**) and (**5**) are affected, resulting in the obvious tendency of hyperchromism and blue shift. The intraligand transition band of the complexes (**2** and **5**) at 293 and 300 nm exhibit hyperchromism of about 50% and 47% with blue shifts of 6 and 10 nm at a ratio of [complex]/[DNA] of 5 respectively. The strong hyperchromism and spectral broadening in absorption intensity indicate interaction of DNA with complexes. For (**3**) and (**6**), the low energy absorption

band at 542 and 537 nm respectively, assigned to metal to ligand charge transfer (MLCT) transition disappeared gradually upon addition of DNA. The initial increase in absorption intensity (hyperchromism 19 and 23%) with a slight blue shift (3 and 6 nm, respectively) is due to electrostatic interaction between DNA and metal complexes. The continuous increase in hyperchromicity of intraligand transition at 296 and 298 nm respectively associated with a spectral shift of 3 and 4 nm to blue shift is typical for an exclusive electrostatic interaction between the complexes and helix surface. For complex **3**, the hyperchromicity approximately attains as high as about 10.2% at the same ratio as complex **6**. The absorption spectrum of all complexes upon titration with DNA did not show any wavelength shift in absorption maxima at 236 nm. However, the addition of DNA clearly yielded an absorbance hyperchromism. There is no special pattern changes in the absorption spectra of the complexes in the presence of DNA have been detected, except increases in hyperchromism for the absorption spectra. This suggests that the interaction between the complexes and DNA should be a weak one between the molecules.

3.6.2. Cyclic voltammetric studies

The cyclic voltammetry is also a useful technique for studying and understanding the binding nature of the metal complexes with DNA. Binding of the complex to the slowly diffusing nucleic acid strand results in decrease in current which is a direct reflection of the concentration of free and bound complex. The decrease of peak current in the presence of DNA implies the interaction of the complexes with DNA. It has already been observed that the new complexes were irreversibly reduced in the range −0.52 to −0.55 V. But, after adding DNA into the complexes, the peak current of the cyclic voltammetric waves diminished regularly, but no palpable change in the peak potential were observed for complexes (**1**), (**2**) and (**4**). However, it can be seen that the cathode peak currents decreased in the presence of DNA. The decrease in current may be attributed to the slow diffusion of an equilibrium mixture of the free and DNA bound complexes to the electrode surface [59]. The decrease in the peak current generally is ascribed to the stronger binding between the complexes and DNA. In contrast, the irregular changes in peak current were observed for the complexes (**3**), (**5**) and (**6**). This indicates the different binding affinity of the complexes with DNA.

3.6.3. Thermal denaturation studies

According to the literature [60,61], the intercalation of natural or synthesized organic- and metallointercalators generally results in a considerable increase in the melting temperature (Tm). The thermal behaviour of DNA in the presence of complexes can give insight into the conformation change as the temperature is raised. The melting temperature Tm of DNA solution, which is defined as the temperature where half of the total base pairs is unbonded, is usually introduced to study the interaction of transition metal complexes with nucleic acid. Generally, the melting temperature of DNA increases when metal complexes bind to DNA by intercalation, as intercalation of the complexes between DNA base pairs causes stabilization of base stacking and hence raises the melting temperature of double-stranded DNA. The melting curves of HS-DNA in the absence and presence of complex are presented in Fig. 4. In the absence of any added complexes, the thermal denaturation carried out for DNA gave a Tm of 60 ± 2 °C under our experimental conditions. We have observed only a minor increase (1–3 °C) in the DNA melting temperature of HS-DNA in the presence of complexes **1–6**, indicating the groove and/or electrostatic binding nature of the complexes. This reveals that the DNA interaction of the present Ru(II) complexes with the double-stranded DNA is relatively weak.

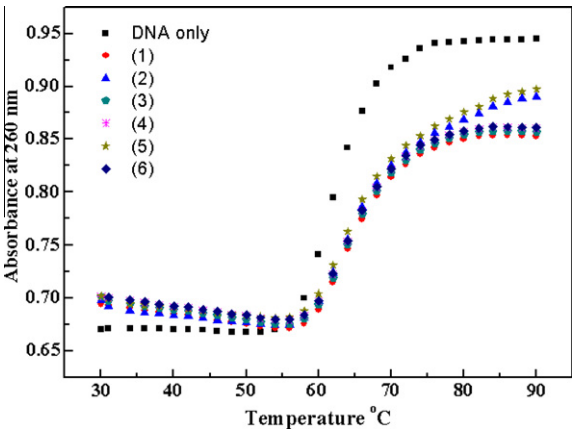

Fig. 4. Thermal denaturation of HS-DNA in the absence and presence of complexes.

3.6.4. Viscosity measurements

The relative change in viscosity was measured using sonicated herring sperm DNA with increasing concentrations of ruthenium compounds. Hydrodynamic measurements sensitive to length change (i.e. viscosity and sedimentation) are regarded as the least ambiguous and most critical tests of a binding mode in solution in the absence of crystallographic structural data [62–64]. The method is based on the well-known fact that intercalation of molecules between DNA bases causes a change in the relative viscosity of solutions due to the unwinding and elongation of the double helix [64–66]. No significant change was observed in the viscosity of DNA for almost all our ruthenium complexes (Fig. 5). From this observation, we can conclude that the complexes may be electro statically bound to the phosphate group of DNA backbone.

3.7. Chemical nuclease activity

There is substantial and continuing interest in DNA endonucleolytic cleavage reactions that are activated by metal ions [67–69]. Redox-active complexes are expected to show good chemical nuclease activity in the presence of metal-based redox couple(s). The cleavage reaction on plasmid DNA can be monitored by agarose gel electrophoresis. When circular plasmid DNA is subjected to electrophoresis, relatively fast migration will be observed for the intact supercoil form (Form I). If scission occurs on one strand (nicking), the supercoil will relax to generate a slower-moving open circular form (Form II). If both strands are cleaved, a linear

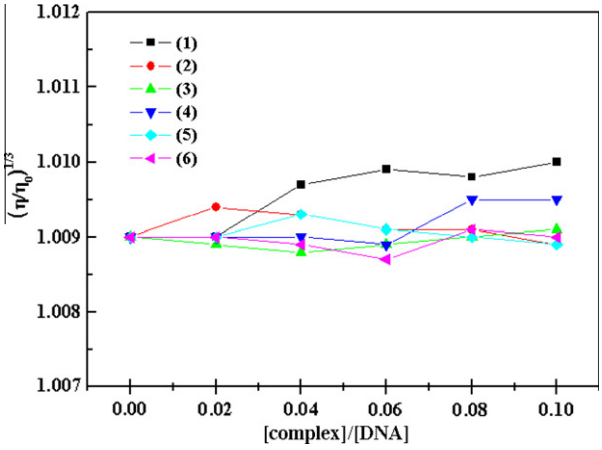

Fig. 5. Effect of increasing amount of the complexes(**1–6**) on the relative viscosity of HS-DNA at 16(±0.1) °C.

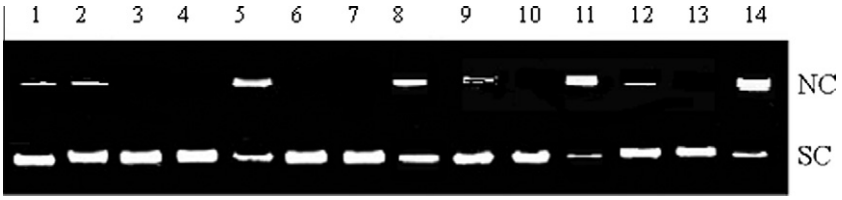

Fig. 6. Cleavage of supercoiled pBR322 DNA by the Ru(II) complexes in Tris–HCl buffer in the presence of sodium ascorbate (1 mM); in TAE buffer at 37 °C. Lane 1, DNA control; lane 2, DNA + sodium ascorbatelane 3, DNA + complex **1** (25 μm); lane 4, DNA + complex **2** (25 μm); lane 5, DNA + complex **3** (25 μm); lane 6, DNA + complex **4** (25 μm); lane 7, DNA + complex **5** (25 μm); lane 8, DNA + complex **6** (25 μm); lane 9, DNA + complex **1** (100 μm); lane 10, DNA + complex **2** (100 μm); lane 11, DNA + complex **3** (100 μm); lane 12, DNA + complex **4** (100 μm); lane 13, DNA + complex **5** (100 μm); lane 14, DNA + complex **6** (100 μm). SC = supercoiled, NC = nicked circular DNA.

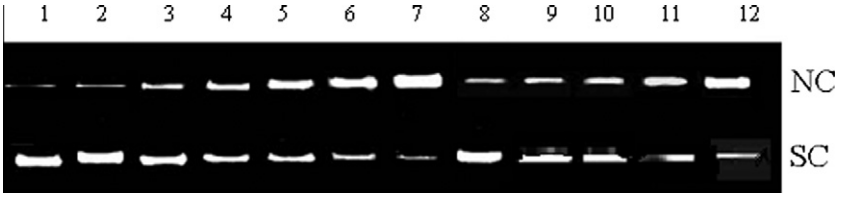

Fig. 7. Cleavage of supercoiled pBR322 DNA by the Ru(II) complexes in Tris–HCl buffer in the presence of sodium ascorbate (1 mM) in TAE buffer at 37 °C. Lane 1, DNA control; lane 2, DNA + sodium ascorbate; lane 3, DNA + complex **3** (20 μm); lane 4, DNA + complex **3** (40 μm); lane 5, DNA + complex **3** (60 μm); lane 6, DNA + complex **3** (80 μm); lane 7, DNA + complex **3** (100 μm); lane 8, DNA + complex **6** (20 μm); lane 9, DNA + complex **6** (40 μm); lane 10, DNA + complex **6** (60 μm); lane 11, DNA + complex **6** (80 μm); lane 12, DNA + complex **6** (100 μm).

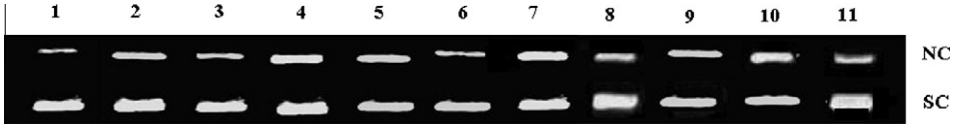

Fig. 8. Cleavage of supercoiled pBR322 DNA by the 40 μm of complex (**3** or **6**) in the presence of sodium ascorbate (1 mM) and potential inhibitors agents. Lane 1, DNA control; lane 2, DNA + complex **3** (40 μm); lane 3, DNA + complex **3** + ethanol (2 mM); lane 4, DNA + complex **3** + NaN_3 (1 mM); lane 5, DNA + complex **3** + tiron (2 mM); lane 6, DNA + complex **3** + KI (5 mM); lane 7, DNA + complex **6**; lane 8, DNA + complex **6** + ethanol (2 mM); lane 9, DNA + complex **6** + NaN_3 (1 mM); 10, DNA + complex **6** + tiron (2 mM); 11, DNA + complex **6** + KI (5 mM).

form (Form III) that migrates between Form I and Form II will be generated [70]. The tests were performed under aerobic conditions with sodium ascorbate (1 mM) as a reducing agent. No cleavage occurs in the absence of sodium ascorbate or with uncomplexed Ru atoms (not shown). As shown in Fig. 6, no obvious DNA cleavage was observed for the control in which metal complex was absent (DNA alone), or incubation of the plasmid with sodium ascorbate alone. The complexes **3** and **6** can effectively cleave DNA but other complexes do not show any significant chemical nuclease activity, even at a concentration as high as 100 μM. It can be concluded that complexes **3** and **6** are the most efficient nuclease in the series. Fig. 7 (lanes 3–8) shows the gel electrophoretic separations of plasmid pBR322 DNA after incubation 24 h in the presence of varying concentrations of complexes **3** and **6** with sodium ascorbate (1 mM). It can be seen that with increasing the concentration of complex, Form II (nicked circular DNA) increase gradually, while Form I (supercoiled circular pBR 322 DNA) diminish gradually, but the Form III (linear DNA) do not occur. It is suggested that these Ru(II) complexes present weak nuclease activity. It is clear that the degradation of pBR 322 DNA is highly dependent on the concentration of complex used. The percentage of Form II demonstrates a linear correlation with concentration. Hence, it is evident that the complexes **3** and **6** in the presence of ascorbate show nuclease activity. The nuclease activity of the **3** and **6** may be related to their different structural features as compared to other complexes.

Reactions in the absence of dioxygen and/or hydrogen peroxide were performed simultaneously. DNA was not cleaved by **3** and **6** under such conditions (not shown). The results indicated molecular oxygen is an essential cofactor for DNA scission and a hydrolytic cleavage mode is not involved. In order to establish the reactive species responsible for the cleavage of the plasmid, the following experiments were carried out. The cleavage activity of **3** and **6** in the presence of different inhibitors are shown in Fig. 8. Complete inhibition of DNA cleavage was observed in the presence of peroxide scavenger such as KI or catalase, which suggests that the peroxide is likely to be the reactive species responsible for the cleavage reaction. Moreover, the cleavage was weakly inhibited by hydroxyl radical scavengers such as ethanol or mannitol. This indicates that $OH^{\cdot}$ may also be the reactive species. However, the cleavage is not inhibited by the singlet oxygen ($^1O_2$) and superoxide dismutase quenchers, suggesting that $^1O_2$ and $O_2^{\cdot-}$ are not the reactive species.

Oxidation of the complexes by molecular oxygen is expected to proceed in a manner analogous to that observed for some ruthenium complexes [71]. The chemical nuclease mechanism of ruthenium complexes was reported rather rarely. A mechanism has been suggested [72,73] involving a simple bimolecular, outer sphere oxidation of the metal ion to generate superoxide, followed by a second single-electron transfer from Ru(II) to yield HO_2^- . In this mechanism the $HO^{\cdot}$ radical produced ultimately is thought to abstract a hydrogen atom from deoxyribose, and lead to sugar fragmentation, base release and then DNA cleavage [74,75].

4. Conclusion

The spectroscopic data and crystal structure of the complexes have been of great help to understanding the uncoordinated oximato oxygen atom. The deprotonation of the oxime OH group leads

to a rearrangement of the electron density from the oxime oxygen to the oxime nitrogen making the latter donor very efficient in metal ion coordination. In addition, the interaction of the complexes with DNA was investigated by absorption spectroscopy, cyclic voltammetry and thermal denaturation measurements. The results indicate that the complexes do not intercalate between the DNA base pairs. Most probably, the interaction of the complexes is mainly electrostatic through the phosphate backbone of the DNA. These results further supported by viscosity measurement. The poor DNA-binding propensity of the complexes could be due to the presence of triphenylphophine as a steric protector ligand. DNA cleavage studies carried out with the complexes demonstrate that the complexes are less efficient in promoting the cleavage of plasmid DNA even in the presence sodium ascorbate. At high concentration, complexes 3 and 6 can effectively cleave the DNA in presence of activating agent.

Supplementary material

CCDC 663251 and 632083 contain the supplementary crystallographic data for **1** and **2**. These data can be obtained free of charge from via http://www.ccdc.cam.ac.uk/conts/retrieving.html, or from the Cambridge Crystallographic Data Centre, 12 Union Road, Cambridge CB2 1EZ, UK; fax: +44 1223 336 033; or e-mail: deposit@ccdc.cam.ac.uk. Supplementary data associated with this article can be found in the online version.

References

[1] V.Y. Kukushkin, D. Tudela, A.J.L. Pombeiro, Coord. Chem. Rev. 156 (1996) 333.
[2] V.Y. Kukushkin, A.J.L. Pombeiro, Coord. Chem. Rev. 181 (1999) 147.
[3] S. Ganguly, S. Karmakar, C.K. Pal, A. Chakravorty, Inorg. Chem. 38 (1999) 5984.
[4] E.A. Bruton, L. Brammer, F.C. Pigge, C.B. Aakeroy, D.S. Leinend, New J. Chem. 27 (2003) 1084.
[5] M. Kurtoglu, S. Serin, Synth. React. Inorg. Met. – Org. Chem. 32 (2002) 629.
[6] M. Ertas, V. Ahsen, A. Gul, O. Bekarogelu, J. Organomet. Chem. 335 (1987) 105.
[7] Y. Gok, H. Kantekin, New J. Chem. 19 (1995) 461.
[8] D.C. Bradley, R.C. Mehrotra, I.P. Rothwell, A. Sing, Alkoxo and Aryloxo Derivatives Metals, Academic Press, London, 2001.
[9] A. Chakravorty, Coord. Chem. Rev. 13 (1974) 1.
[10] A.M. Duda, A. Karaczyn, H. Kozlowski, I.O. Fritsky, T. Glowiak, E.V. Prisyazhnaya, T.Y. Sliva, J.S. Kozlowskac, J. Chem. Soc. Dalton Trans. 3853 (1997).
[11] B. Kurzak, H. Kozlowski, E. Farkas, Coord. Chem. Rev. 114 (1992) 169.
[12] B. Cervera, R. Ruiz, F. Lloret, M. Julve, J. Faus, M.C. Munoz, Y. Journaux, Inorg. Chim. Acta 288 (1999) 57.
[13] R. Ruiz, J. Sanz, B. Cervera, F. Lloret, M. Julve, C. Bois, J. Faus, M. Carmen Munoz, J. Chem. Soc. Dalton Trans. 1623 (1993).
[14] M. Kandaz, I. Yylmaz, S. Keskin, A. Koca, Polyhedron 21 (2002) 825.
[15] J.R. Dilworth, S.J. Parrott, Chem. Soc. Rev. 27 (1998) 43.
[16] P.J. Blower, Trans. Met. Chem. 23 (1998) 109.
[17] W.A. Wolkert, T.J. Hoffman, Chem. Rev. 99 (1999) 2269.
[18] K. Ohta, R. Higashi, M. Ikejima, I. Yamamoto, N. Kobayashi, J. Mater. Chem. 8 (1998) 1979.
[19] B.G. Malmstrom, Acc. Chem. Res. 26 (1993) 332.
[20] M.C.M. Laranleira, R.A. Marusak, A.G. Lappin, Inorg. Chim. Acta 186 (2000) 300.
[21] M. Bakir, J. Electroanal. Chem. 466 (1999) 60.
[22] M. Bakir, J.A.M. McKenzie, J. Chem. Soc. Dalton Trans. 3571 (1997).
[23] A.R. Ozkaya, A. Gurek, A. Gul, O. Bekaroglu, Polyhedron 16 (1997) 1877.
[24] A.R. Ozkaya, I. Yilmaz, O. Bekaroglu, J. Porphyrins, Phthalocyanines 2 (1998) 483.
[25] A.R. Ozkaya, E. Hamuryudan, Z. Altuntas¸ Bayyr, O. Bekaroglu, J. Porphyrins Phthalocyanines 4 (2000) 689.
[26] D. Mansuy, P. Battioni, J.-P. Battioni, Eur. J. Biochem. 184 (1989) 267.
[27] J. Custot, J.-L. Boucher, S. Vadon, C. Guedes, S. Dijols, M. Delaforge, D. Mansuy, J. Biol. Inorg. Chem. 1 (1995) 73.
[28] A.I. Vogel, Text Book of Practical Organic Chemistry, 5th ed., Longman, London, 1989.
[29] N. Ahmed, J.J. Lewison, S.D. Robinson, M.F. Uttley, Inorg. Synth. 15 (1974) 48.
[30] R.A.S. Pelgado, W.Y. Lee, S.R. Choi, Y. Cho, M.J. Jun, Trans. Met. Chem. 16 (1991) 241.
[31] Bruker Advanced X-ray Solutions SMART for WNT/2000, Version 5.628, Bruker AXS Inc., Madison, Wisconsin, USA, 1997–2002.
[32] Bruker Advanced X-ray Solutions SAINT, Version 6.45, Bruker AXS Inc., Madison, Wisconsin, USA, 1997–2003.
[33] Bruker Advanced X-ray Solutions SADABS in SAINT, Version 6.45, Bruker AXS Inc., Madison, Wisconsin, USA, 1997-2003.
[34] G.M. Sheldrick, SHELXTL, Version 6.14, Bruker AXS, Inc, Madison, WI, 2003.
[35] S.C. Jakels, F. Farmery, E.K. Barfield N.J. Rose, D.H. Busch, Inorg. Chem. 11 (1972) 289.
[36] M.A. Greaney, C.L. Coyle, M.A. Harmer, A. Jordan, E.I. Stifel, Inorg. Chem. 28 (1989) 912.
[37] E.S. Dodsworth, A.B.P. Lever, Chem. Phys. Lett. 124 (1986) 152.
[38] A. Cukurovali, E. Tas, Synth. React. Inorg. Met. – Org. Chem. 28 (3) (1998) 449.
[39] L.A. Epps, L.G. Marzilli, Inorg. Chem. 12 (1973) 1514.
[40] A.L. Crumbliss, P.L. Gaus, Inorg. Chem. 14 (11) (1975) 2745.
[41] L.F. Szczepura, J.G. Muller, C.A. Bessel, R.F. See, T.S. Janik, M.R. Churchill, K.J. Takeuchi, Inorg. Chem. 31 (1992) 859.
[42] N. Chitrapriya, V. Mahalingam, L.C. Channels, M. Zeller, F.R. Fronczek, K. Natarajan, Inorg. Chim. Acta 361 (2008) 2841.
[43] R. Raveendran, S. Pal, Polyhedron 24 (2005) 57.
[44] M. Maji, M. Chatterjee, S. Ghosh, S.K. Chattopadhyay, B.-M. Wu, T.C.W. Mak, J. Chem. Soc. Dalton Trans. 135 (1999).
[45] N. Chitrapriya, V. Mahalingam, M. Zeller, K. Natarajan, Polyhedron 27 (2008) 1573.
[46] E. Bermejo, A. Castineiras, D.X. West, Z. Naturforsch. 56B (2001) 369.
[47] J.D. Martin, K.A. Abboud, K.-H. Dahmen, Inorg. Chem. 37 (1998) 5811.
[48] S. Ganguly, V. Manivannan, A. Chakravorty, J. Chem. Soc. Dalton Trans. 146 (1998).
[49] S.A. Serron, C.M. Haar, S.P. Nolan, Organometallics 16 (1997) 5120.
[50] M. Poyatos, J.A. Mata, E. Falomir, R.H. Crabtree, E. Peris, Organometallics 22 (2003) 1110.
[51] M.A. Rankin, R. McDonald, M.J. Ferguson, M. Stradiotto, Angew. Chem. Int. Ed. 44 (2005) 3603.
[52] M. Calleri, G. Ferreris, D. Viterbo, Acta Crystallogr. 20 (1966) 73.
[53] L.E. Sutton, Spec. Publ. – Chem. Soc. 18 (1965).
[54] S.M. Morehouse, A. Polychronopoulou, G.J.B. Williams, Inorg. Chem. 19 (1980) 3558.
[55] Z.D. Xu, H. Liu, S.L. Xiao, M. Yang, X.H. Bu, J. Inorg. Biochem. 90 (2002) 83.
[56] Y. Wang, Z.-Y. Yang, Trans. Met. Chem. 30 (2005) 902.
[57] C.-Y. Zhou, J. Zhao, Y.-B. Wu, C.-X. Yin, P. Yang, J. Inorg. Biochem. 101 (2007) 10.
[58] Q.S. Li, P. Yang, H.F. Wang, M.L. Guo, J. Inorg. Biochem. 64 (1996) 181.
[59] J. Liu, T. Zhang, T. Lu, L. Qu, H. Zhou, Q. Zhang, L. Ji, J. Inorg. Biochem. 91 (2002) 269.
[60] M.J. Waring, J. Mol. Biol. 13 (1965) 269.
[61] G.A. Neyhart, N. Grover, S.R. Smith, W.A. Kalsbeck, T.A. Fairly, M. Cory, H.H. Thorp, J. Am. Chem. Soc. 115 (1993) 4423.
[62] X. Xiaoli, Y. Manman, Z. Chengyong, Z. Jing, Y. Pin, Chin. Sci. Bull. 51 (19) (2006) 2322.
[63] D.S. Sigman, A. Mazumder, D.M. Perrin, Chem. Rev. 93 (1993) 2295.
[64] S. Satyanarayana, J.C. Dabrowiak, J.B. Chaires, Biochem. 31 (1992) 9319.
[65] J.B. Suh, Chaires, Bioorg. Med. Chem. 3 (6) (1995) 723.
[66] J.D. Aguirre, A.M. Angeles-Boza, A. Chouai, C. Turro, J. Pellois, K.R. Dunbar, Dalton Trans. (2009) 10806.
[67] D.S. Sigman, Acc. Chem. Res. 19 (1986) 180.
[68] B. Armitage, Chem. Rev. 98 (1998) 1171.
[69] A. Sitlani, E.C. Long, A.M. Pyle, J.K. Barton, J. Am. Chem. Soc. 114 (1992) 2303.
[70] J.K. Barton, A.L. Raphael, J. Am. Chem. Soc. 106 (1984) 2466.
[71] D. Stanbury, O. Haas, H. Taube, Inorg. Chem. 19 (1980) 518.
[72] P. Uma Maheswari, M. Palaniandavar, J. Inorg. Biochem. 98 (2004) 219.
[73] P. Uma Maheswari, M. Palaniandavar, Inorg. Chim. Acta 357 (2004) 901.
[74] R.P. Hertzberg, P.B. Dervan, J. Am. Chem. Soc. 104 (1982) 313.
[75] R.P. Hertzberg, P.B. Dervan, Biochemistry 23 (1984) 3934.